Time-dependent magnetospheric configuration and breakup mapping during a substorm

M. Kubyshkina,[1] V. Sergeev,[1] N. Tsyganenko,[1] V. Angelopoulos,[2] A. Runov,[2] E. Donovan,[3] H. Singer,[4] U. Auster,[5] and W. Baumjohann[6]

Received 30 June 2010; revised 22 October 2010; accepted 3 November 2010; published 4 February 2011.

[1] We analyze an isolated substorm on 29 March 2009 observed by the Thermal Emission Imaging System (THEMIS) and well monitored by ground-based observatories at and near station Gillam. The event provides a rare opportunity for monitoring the substorm magnetic topology thanks to fortuitous clustering of the THEMIS probes, complemented by the GOES 12 spacecraft. The neutral sheet position was found to be displaced by ~0.5 R_E northward from its average location. The peak cross-tail current density was estimated to be ~20 nA/m^2 at the end of the growth phase, revealing the formation of a thin current sheet during the last 15 min prior to the expansion onset. The fortuitous spacecraft conjunction allowed us to construct an adjusted time-varying model based on magnetic field and pressure observations during the substorm. We then used the adjusted model to map the location of the spacecraft to the ionosphere and the breakup from the ionosphere to the equatorial region. Significant time-dependent differences between this and the standard models (e.g., T96) do exist, resulting in breakup mapping to ~22 R_E, compared to 12 R_E if classical models are used. Moreover, we find that spacecraft footprints in the ionosphere move significantly equatorward (2°) over tens of minutes during the growth phase but jump poleward (2°–4°) after expansion onset. Since such motions are also typical for auroral arcs during substorms, we infer that magnetic field reconfiguration during various substorm phases, rather than plasma motion in the equatorial magnetosphere, is largely responsible for the observed motion of the aurora.

Citation: Kubyshkina, M., V. Sergeev, N. Tsyganenko, V. Angelopoulos, A. Runov, E. Donovan, H. Singer, U. Auster, and W. Baumjohann (2011), Time-dependent magnetospheric configuration and breakup mapping during a substorm, *J. Geophys. Res.*, *116*, A00I27, doi:10.1029/2010JA015882.

1. Introduction

[2] Substorm development in the magnetosphere and corresponding magnetic field changes have been extensively studied during the era of spacecraft observations, and the major features are believed to be well understood. Among those common for each substorm are lobe field enhancement (hence tail current intensification) during the growth phase, and subsequent rapid field (and current) decrease during the expansion phase, accompanied by the change in a magnetic field topology to a more dipole-like configuration. Also, many substorm-related studies imply a development of a thin current sheet, embedded within a plasma sheet prior to substorm expansion [see *Birn et al.*, 2003; *Sergeev et al.*, 1993; *Sanny et al.*, 1994, and references therein]. At the same time, standard empirical field models (T89, T96, T01, see [*Tsyganenko*, 1989, 1995, 2002a, 2002b]) cannot reproduce the rapid substorm-related evolution of the magnetosphere. Because these models are derived from large data sets, they can only reflect average trends during periods with changing interplanetary conditions.

[3] A special approach to explore the field and current evolution during a substorm growth phase was first introduced by *Pulkkinen* [1991]. That approach used a modified version of the T89 model, which included a few free parameters and allowed alteration of the model currents by changing their intensity, position, and thickness. These quantities were treated as free parameters whose values were obtained from observations made during a particular substorm event; in later works this approach was termed "event-oriented modeling." Although magnetic fields obtained in that modified model were much closer to observations, the

[1]Institute of Physics, Saint Petersburg State University, St. Petersburg, Russia.
[2]Institute of Geophysics and Planetary Physics, University of California, Los Angeles, California, USA.
[3]Department of Physics and Astronomy, University of Calgary, Calgary, Alberta, Canada.
[4]NOAA Space Weather Prediction Center, Boulder, Colorado, USA.
[5]Institut für Geophysik und Extraterrestrische Physik der Technischen Universitaet Braunschweig, Braunschweig, Germany.
[6]Space Research Institute, Austrian Academy of Sciences, Graz, Austria.

0148-0227/11/2010JA015882

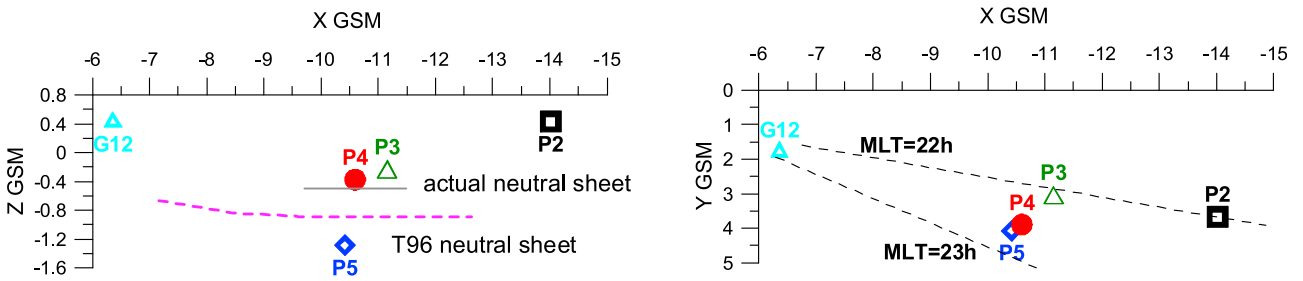

Figure 1. Spacecraft location during the 29 March 2009 substorm event. (left) X_{GSM} versus Z_{GSM} plane with estimation of neutral sheet position from observations (black line) and from T96 model (dashed purple line). (right) X_{GSM} versus Y_{GSM} plane.

approach had a number of limitations. The most critical one was the lack of events, in which observations were made by several spacecraft, located in the same local time sector but at different radial distances in the range of 6–20 R_E, which made it difficult to constrain the model parameters. The other problem was a tedious procedure of defining free parameters from a small number of observational data. Therefore the approach was not widely applied. Several modeled cases [*Pulkkinen et al.*, 1991, 1994a, 1994b] showed a similar reconfiguration of the magnetic field and current during the substorms.

[4] The *Pulkkinen* [1991] approach was later extended to use not only the magnetic field data but also the isotropic boundary positions, plasma pressure, and temperature anisotropy [*Kubyshkina et al.*, 1999, 2002; *Sergeev et al.*, 2005, 2007; *Pulkkinen et al.*, 2006]. It was also modified to use the T96 rather than the T89 model [*Lu et al.*, 1999; *Kubyshkina et al.*, 2008]. In the modeled substorm events, similar variations of currents during the growth phase were obtained, i.e., intensification of the tail and ring currents and formation of a thin current sheet between 8 and 20 R_E. Although the degree of current intensification and the parameters of thin current sheet varied from substorm to substorm, in all cases the magnetic field changed to a more stretched configuration, in which the auroral breakup footprint mapped to the region with stretched field lines (thin current sheet).

[5] When mapping the breakup location from the ionosphere to the plasma sheet, some authors [see, e.g., *Elphinstone et al.*, 1991; *Wanliss*, 2006, and references therein] use standard Tsyganenko models, without taking into account the transient stretching of the nightside field. As a result, they conclude that the substorm source region lies in the inner magnetosphere.

[6] By contrast, previously developed event-oriented models use spacecraft observations from individual events to reconstruct field configuration for a given substorm [*Kubyshkina et al.*, 2002, 2009; *Sergeev et al.*, 2005]. These models map breakup latitudes to much greater tailward distances; in various events these estimations map the breakup to R ≈ 15–27 R_E. This result cannot be considered statistically meaningful, however, because the number of modeled cases is too small. In addition, the model neutral sheet position may be different from the actual one, which could cause errors in data interpretation, and in many cases it was impossible to determine the neutral sheet position from observations.

[7] To further investigate these questions, we carried out a detailed study of a moderate substorm on 29 March 2009, when the spacecraft location was extremely favorable for data-based modeling, and a detailed picture of the substorm evolution was available from the Gillam ground-based observatory.

[8] One of the goals of this work is to evaluate the difference in the mapping of a breakup to the magnetosphere using various models and to assess the effect of thin current sheet parameters on mapping results. To that end, we constructed a time-varying model of a substorm, checked its quality (checking the standard model results at the same time) and then compared the mapping results using both models.

2. Observations

[9] A very detailed description of observations on 29 March 2009 is given in the companion paper [*Sergeev et al.*, 2010] (hereafter referred to as paper 1); therefore, we concentrate mostly on the points important for our study. We analyze the available spacecraft positions presented in Figure 1 and the observed magnetic fields variations (Figure 2).

[10] During the moderate substorm on 29 March 2009, with a growth phase starting around 0430 UT, we have observations of four Time History of Events and Macroscale Interactions during Substorms (THEMIS) probes, grouped at distances from −10 R_E to −14 R_E within a 1 h wide local time sector. Two probes P4 and P5, located at the same longitude and equatorial distance, were separated by ~1 R_E distance in the Z_{GSM} direction; such a configuration allows us to estimate the portion of current embraced by two probes at a given distance. P3 is quite close to P4 and slightly shifted to the north, which makes it possible to estimate the current density at these distances. Additionally, P2 is farther down the tail and a GOES 12 satellite is at geosynchronous orbit, which allows us to control the radial distribution of magnetic field (and, hence, currents) in the magnetotail.

[11] As we see, in this event spacecraft location is almost perfect for constructing an event-oriented substorm model. Yet probably the most important fact is that the tangential to the neutral sheet (B_x) component at P4 probe (red line) remains virtually zero during the entire growth phase, which means that P4 stays in the center of the neutral sheet. Usually, when modeling the magnetic field, it is impossible to accurately determine from data the neutral sheet position, a crucial parameter for a model; this event is a serendipitous exception. We also would like to note that the statistical position of the neutral sheet for that specific date/time and observed solar wind parameters [*Tsyganenko and Fairfield*,

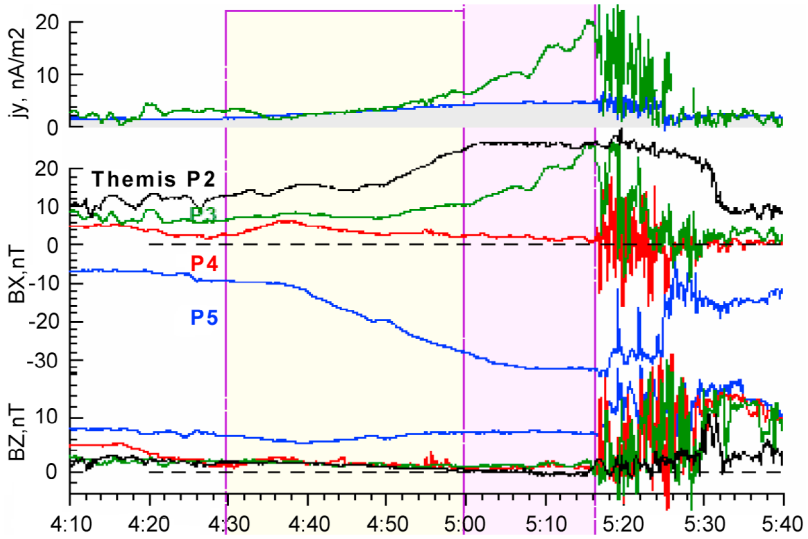

Figure 2. (bottom) B_x and B_z magnetic fields components observed by THEMIS probes P2, P3, P4 and P5. (top) Current density near P4 and P3 obtained from the difference in corresponding B_x values.

2004] should lie halfway between P4 and P5, as shown by purple dashed line in Figure 1 (left).

[12] From magnetic field observations by THEMIS probes [*Auster et al.*, 2008] one may also notice (Figure 2) that the growth phase may be divided into two periods: (1) from 0430 to 0500 UT, when B_x increases on both P2 and P5 (Figure 2, black and blue lines, respectively), demonstrating growing lobe magnetic flux and total tail current, and (2) after 0500 and through the start of the expansion, when the lobe field remains nearly constant at both probes. By contrast, during this second period the B_x component at P3 (located in the vicinity of the neutral sheet, slightly above P4) starts to increase rapidly, revealing the current density enhancement near the neutral sheet. This kind of behavior (constant total integrated current and increasing current density) may be interpreted as formation of a thin current sheet in the center of the plasma sheet near P4 and P3.

[13] Furthermore, we can get a crude estimate of current density by comparing the values of B_x, measured by P4 and P3 as

$$j_y \sim c/4\pi(B_{x_{P3}} - B_{x_{P4}})/\Delta Z,$$

where ΔZ is the Z_{GSM} separation between P3 and P4. The j_y thus calculated is shown in Figure 2, from which one sees that the maximal current density reaches there 20 nA/m^2.

[14] Similar estimates for the integral current can be obtained as

$$J_{int}(z) \sim 2c/4\pi \int_{z_{ns}}^{z} \frac{\partial B_x}{\partial z'}(z')dz' \sim 2c/4\pi B_x(z),$$

from which the integral current at P2 and P5 equals ~4.4 × 10^7 nA/m, and ~6.1 × 10^7 nA/m, respectively. This equation demonstrates interesting observational facts that could be obtained from an event-oriented model and that serve as a test of the model's accuracy.

3. Time-Dependent Magnetic Field Model With a Thin Current Sheet

[15] The adapted time-dependent models were introduced by *Kubyshkina et al.* [2009] (hereafter referred to as paper 2), which focused on versions AM01 and AM02, with the AM03 version mentioned briefly. This section contains a brief synopsis of the AM01 and AM02 models (described in details in paper 2) and then concentrates in more detail on the AM03 version. The main features of each version, which is discussed here, are summarized in Table 1 (adapted and revised from paper 2).

Table 1. Different Versions of Adaptive Models

Version	Input Data	Parameters Varied (Parameters Predefined)	Problems Detected
AM-01	magnetic field observations on THEMIS only	input parameters for T96 (parmod(1:4)	often overstretched
AM-02	version 01 input data + magnetic field observations form other spacecraft available in the nearby local time sector + plasma pressure for distant THEMIS (and Geotail if available)	parmod(1,2,4) + additional rotation of a neutral sheet from Sun-Earth radial direction (parmod(3) is taken from SW observations)	often understretched and underestimate the tail current
AM-03	version 02 input data + plasma pressure (if available and well determined) + isotropic boundaries (if available)	intensity and thickness of additional thin current sheet + intensity of T96 basic ring and tail current systems + additional rotation (parmod(1,2,3,4) are taken from AM02)	under consideration

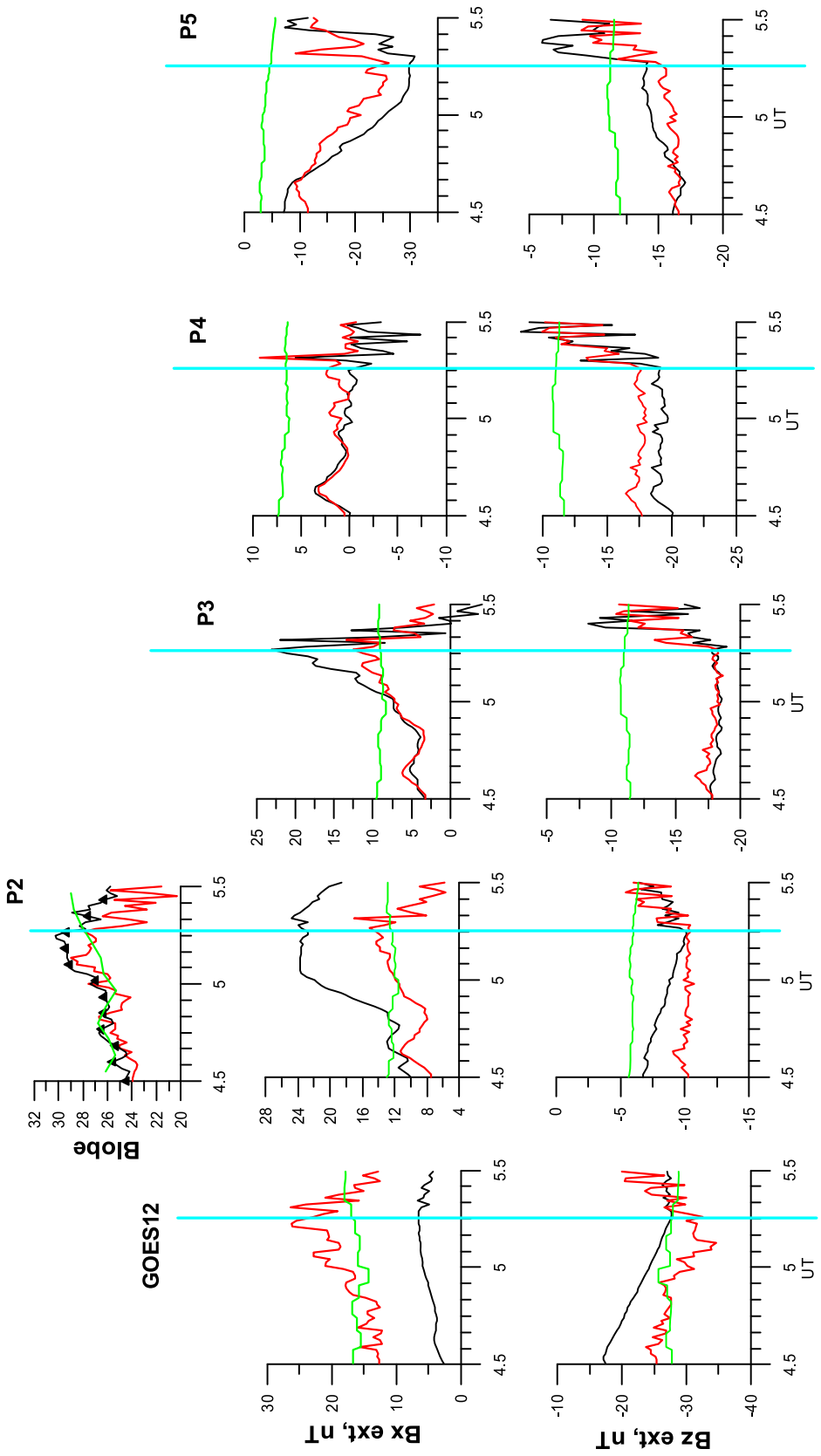

Figure 3. The external part of the observed B_x and B_z magnetic field components (black lines) together with the predictions of standard T96sw (green lines) and AM03 (red lines) models. Vertical light blue lines represent the substorm onset time.

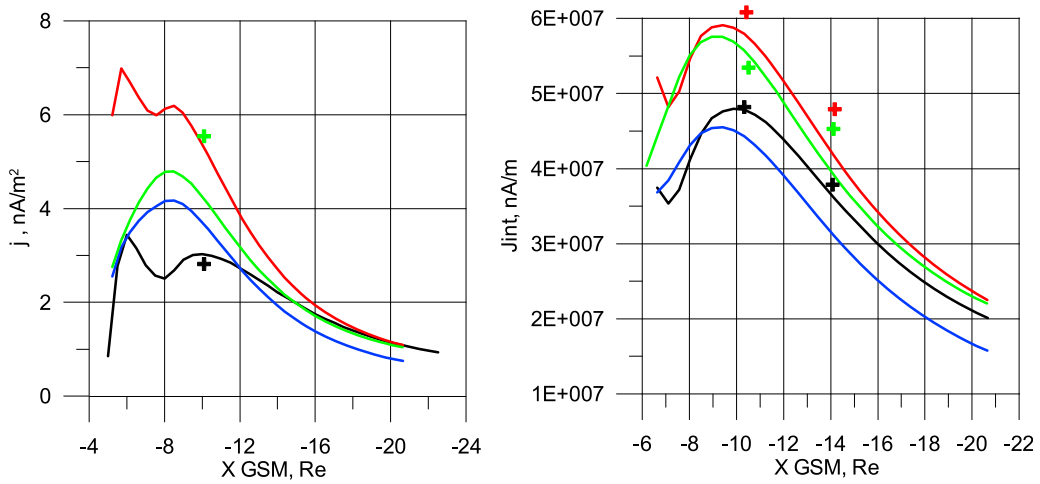

Figure 4. (left) Current density distribution along neutral sheet in the 22.5 MLT meridian for four consequent times: 0455 UT, end of first part of growth phase, black line; 0505 UT, start of second part of growth phase, green line; 0515 UT, end of growth phase, red line; and 0524 UT, after the onset, blue line. Rough estimates of current density obtained from magnetic field observed by THEMIS probes P5 and P4 near X_{GSM} = 10 R_E for 0455 and 0505 UT are shown as crosses of corresponding color. (right) The same for integral current density. Here the observational estimates of integral current were made for P5 and P2, i.e., at X_{GSM} ($P5$) = 10 R_E and X_{GSM} ($P2$) = 14 R_E) for 0455, 0505, and 0515 UT.

[16] The AM01 adaptive model is based on a standard T96 field with its input parameters (solar wind ram pressure, IMF B_y and B_z, and SymH index) varied to minimize the RMS deviation between the model field and that observed by THEMIS. Note that the internal structure of the T96 model remains intact in that simplest version. The AM02 version differs from AM01 in that (1) it uses not only the magnetic field data but also the observed total pressure (or the tail lobe magnetic field) and (2) the model neutral sheet is allowed to be rotated in the XZ plane (following, for example, the solar wind direction). Both versions can be run routinely to represent the magnetospheric configuration for long periods of time, as they do not change the internal structure of the T96 current systems and do not include many free parameters (4 and 5, respectively). As discussed in paper 2, both versions may provide a fair approximation to real magnetic field configurations; although the AM01 version may be somewhat overstretched, and the AM02 version may be understretched and underestimate the tail current.

[17] To obtain an even more accurate reconstruction of the current systems during a substorm, one needs to include variations of model currents in addition to those already present in T96. This is implemented in the most advanced version of adaptive models, AM03. Its main difference from T96 is that we add one more current sheet with the same structure as the original T96 tail current (short mode, confined within 20 R_E) but with variable thickness and intensity, which adds two more free parameters to be determined from data. Having added the extra current sheet, we need to allow the magnitudes of basic T96 currents (ring current and two modes of tail currents) to be varied. In addition, the AM03 model includes a variable direction of tail field stretching, which is often different from the Sun-Earth line. In total, the AM03 version has 6 free parameters.

[18] One more peculiarity of the adaptive AM03 model is that it is constructed in two steps: (1) specifying parameters of the AM02 version for a given event, which provides best-fit values of the background T96 field input parameters, and (2) adding the extra tail current and varying its intensity and thickness in combination with varying the tilt of the entire tail current. To obtain the six free parameters of the model, we use magnetometer data from all available spacecraft, together with the total pressure (magnetic and plasma) at the distant ($R > 13R_E$) spacecraft as a proxy for the lobe field at a given distance (assuming transverse pressure balance across the tail). The error function to be minimized is the same as that introduced in paper 2:

$$B_{Err} = \frac{1}{W_T}\sum_{i=1}^{N} W_i \sqrt{\left((B_{OXi}-B_{MX_i})^2+(B_{OY_i}-B_{MY_i})^2+(B_{OZ_i}-B_{MZ_i})^2\right)} + \frac{1}{N_{lobe}}\sum_{i=1}^{N_{lobe}} \sqrt{(B_{lobe_{Oi}}-B_{lobe_{Mi}})^2}, \quad (1)$$

where W_i are weight factors, generally different for each spacecraft, and the total weight $W_T = \sum_i W_i$ indicates the number of spacecraft included in modeling. Using the weight factors helps control the spatial coverage, as well as the importance or reliability of particular spacecraft. Normally all W_i are equal unity, unless explicitly specified otherwise. The search of free parameters on the second step is done with a combination of Monte Carlo and gradient search methods within the specified range of free parameters change.

4. Results and Discussion

4.1. Fields and Currents in the Resulting Model

[19] The resulting external (with IGRF subtracted) magnetic field as reproduced by the AM03 model (Figure 3, red

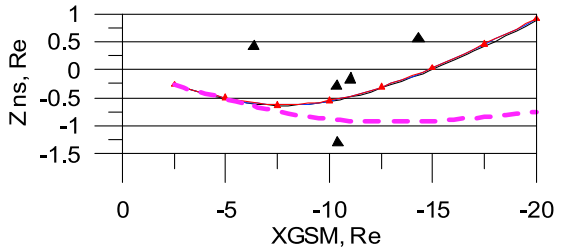

Figure 5. Neutral sheet position for the same times as in Figure 4 (here the lines almost coincide); triangles mark THEMIS probes positions.

line) at locations of all spacecraft with data entered in the modeling data set is shown in Figure 3 together with observations (black line) and the standard T96 model output (green line). The light blue line indicates the time of substorm onset. The observed B_{lobe}, entering in (1), was calculated from

$$B_L(x,y) = \sqrt{\left[2\mu_0 P + \left(B_x^2 + B_y^2 + B_z^2\right)\right]},$$

where P and B_x, B_y, B_z are the plasma pressure and the magnetic field components measured by a spacecraft in the midtail plasma sheet or in the lobe. The equivalent lobe field B_{lobe_m} was computed from the model at a point(x, y) located 5 R_E north (or south) of the neutral sheet position, which was derived from the model. Also, to provide better representation of neutral sheet location, which is dictated by zero magnetic field at P4 THEMIS probe, we increased the weight of P4 data twice, making it equal to 2, whereas weights of all other spacecraft were taken equal to 1.

[20] From Figure 3 one may see that agreement of the AM03 model with observations is much better than that of T96 for all THEMIS probes. The agreement is very good for both B_x and B_z at P3, P4 and P5 (least squares deviation, σ^2, for each spacecraft for both components is less than 2.0 nT during the period); it is satisfactory in B_z at GOES (σ^2 = 5 nT, which is 20% of the mean value) and at P2 (σ^2 = 2 nT, which is 20% of the mean value); and it is somewhat worse for B_x at GOES (σ^2 = 11 nT), and P2 (σ^2 = 6 nT). It is interesting to note that at P2 the AM03 model underestimates B_x (though the behavior is similar), and at GOES B_x is overestimated by the model. The fact that the model and the observed field are close to each other (average error for all spacecraft does not exceed 7 nT throughout the entire period) proves that the modeled current distribution is close to the real one. With a time-varying model of the magnetic field, we may explore the temporal and spatial variations of cross-tail current during a substorm and compare the results with facts derived directly from observations.

[21] Figure 4 shows spatial variation of the current density, integral current, neutral sheet position and B_z in the neutral sheet in the 22.5 MLT meridian for four consequent times: 0455 UT (end of the first part of the growth phase), 0505 UT (start of the second part of the growth

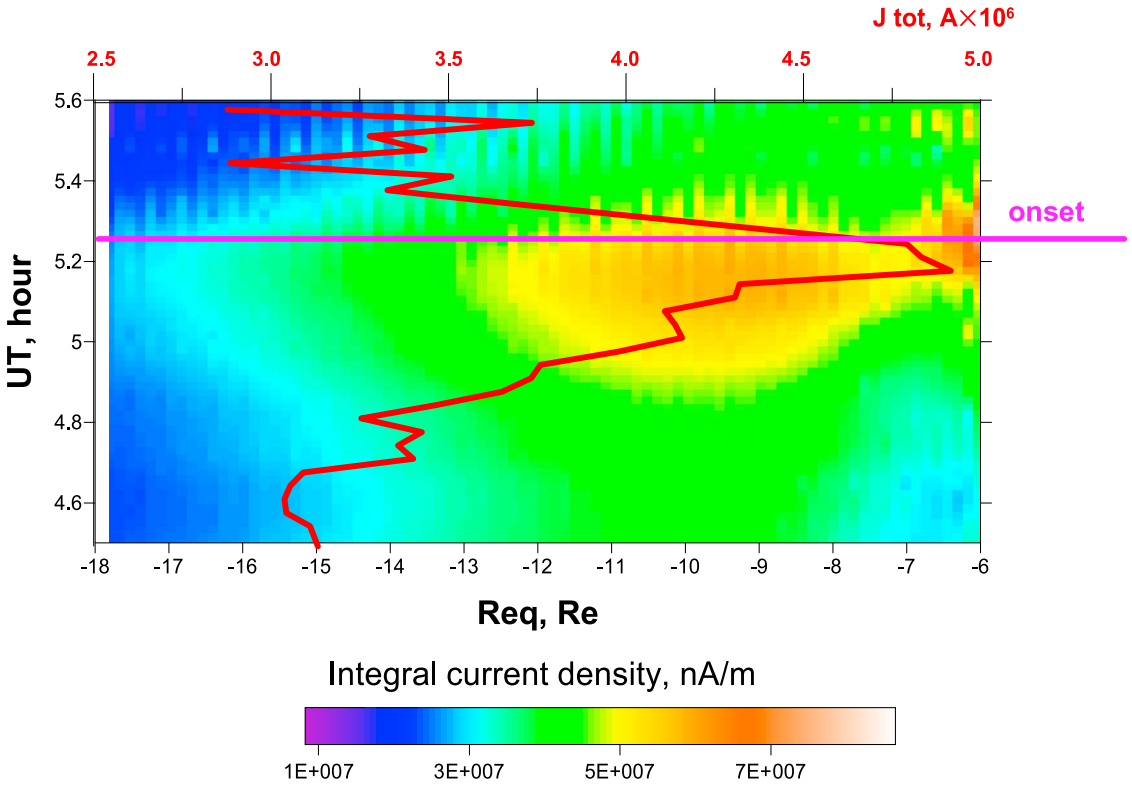

Figure 6. The integral current density radial distribution for the 22.5 MLT meridian during the substorm. The red curve gives the time changes of the total current, between −4 and −17 R_E.

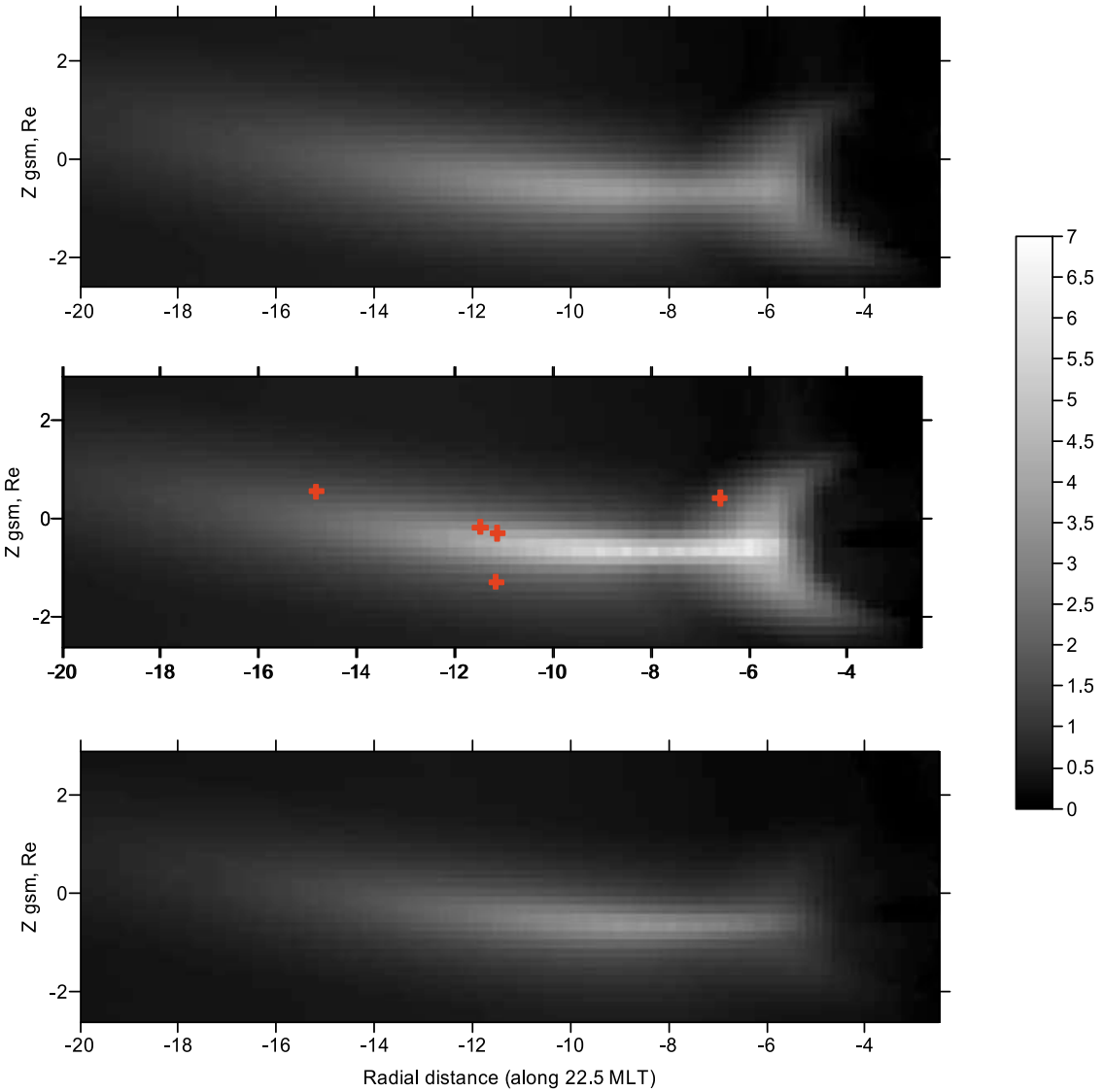

Figure 7. Current density radial distribution for 22.5 MLT at three different times: (top) 0500 UT (end of early growth phase), (middle) 0515 UT (end of late growth phase), and (bottom) 0524 UT (after onset). Red crosses on Figure 7 (middle) show probe positions.

phase), 0515 UT (end of the growth phase), and 0524 UT (7 min after the onset).

[22] Although the current density in the midtail gradually increases during the growth phase, its maximum value (7 nA/m^2) is less than that estimated from observations for the late growth phase (18 nA/m^2, see the difference in the observed and modeled B_x at P3 during the last minutes of the growth phase, Figure 2). After the breakup at ~0516/17 UT (see paper 1), the current density reduces to its normal values. The integral current density (i.e., the total current per unit tail length) behaves in a different way: in accordance with observations, it grows during the early growth phase to the estimated values of 6×10^7 nA/m near 10 R_E (P5) and 4.2×10^7 nA/m at 14 R_E (P2). From 0505 UT until onset it remains almost constant. This result shows that although we correctly estimate the total current in the plasma sheet at distances 10–14 R_E, we underestimate the intensity (or overestimate the thickness) of the embedded thin current sheet. One reason could be inaccurate placing of the thin current sheet, which in our model overlies the basic T96 short-mode tail current [*Tsyganenko*, 1995].

[23] Figure 5 shows the positions of the neutral sheet for the same times; triangles mark probe locations; the purple dashed line shows the standard T96 neutral sheet location. One can see that the neutral sheet location does not change with time in the AM03 model, but it differs considerably from a statistical neutral sheet location in standard models: at the P4 distance it is shifted northward by 0.5 R_E towards P4, which also agrees with observations.

[24] We conclude that the resulting AM03 model agrees well with most of available observations and may be used to describe the time-varying structure of the tail current during the substorm sequence. A global view of the dynamical current distribution is shown in Figures 6 and 7. The radial distribution of the integral current for the 22.5 MLT

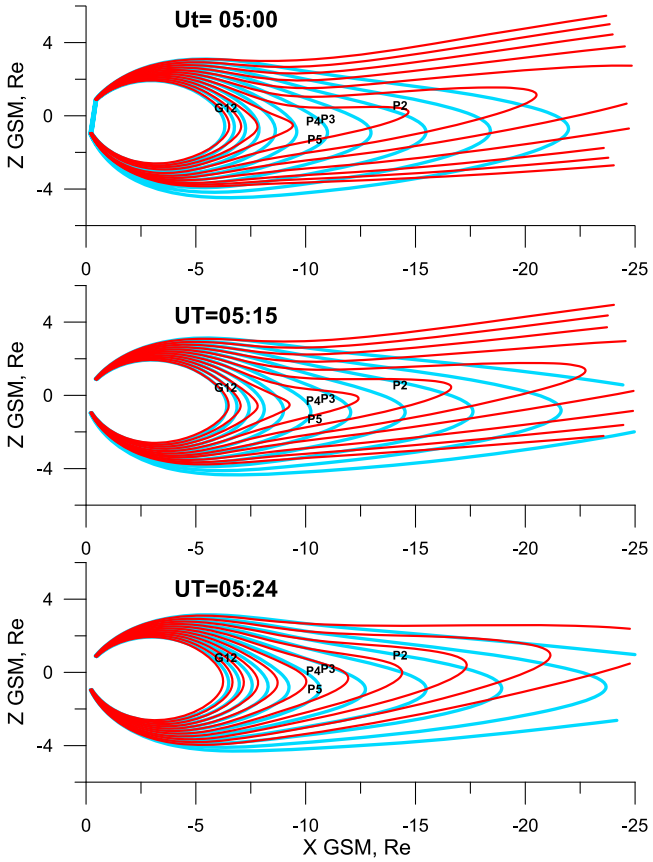

Figure 8. Field lines configuration at 22.5 MLT meridian for three time moments (same as in Figure 7) for AM03 (red lines) and T96 (blue lines).

meridian during the substorm in Figure 6 demonstrates its gradual increase during the growth phase (by ~20% above the T96 values) and fast disruption of the current after the onset. An interesting feature is that according to the model, the inner edge of the intense current moves towards Earth by about 1 R_E during the substorm; this motion is more pronounced during the second period of the growth phase.

[25] Figure 7 shows the spatial distribution of the current density at three moments: 0500 UT (end of early growth phase), 0515 UT (end of late growth phase), and 0524 UT (after onset). Red crosses in the Figure 7 (middle) show spacecraft positions. Note formation of a thin current sheet with a thickness of ~0.1 R_E. The current density increases twice after the formation of the thin current sheet (Figure 7, middle) and returns to lower values after it disappears. The most intense currents are located at distances 6 ÷ 12 R_E and the three THEMIS probes remain at the tailward end of that region. The neutral sheet is shifted upward from the equatorial plane, which is consistent with P4 data and with the observed direction of the solar wind flow, which had a positive V_z (see paper 1).

[26] In addition to electric current structure, an important issue is the configuration of magnetic field lines connecting the spacecraft to the ionosphere, which is directly related to the interpretation of ground observations. Based on the fact that the magnetic fields are significantly different in the standard T96 and AM03 models, one may expect that the field line configurations will also be quite different. Figure 8 compares the model field lines at the LT = 22.5 MLT meridian for the same three time moments as in Figure 7.

[27] The innermost field line in Figure 8 has its footprint at 65.5° of corrected geomagnetic latitude (CGL, introduced by *Hultqvist and Gustafsson* [1960]); the next 11 field line footprints are 0.5° apart. Due to much stronger stretching and additional shift of the plasma sheet, the relative positions of spacecraft and the magnetic field differ in the two models. For example, P5 and P2 are nearly on the same field line in AM03, whereas according to the T96 model the P5 would remain on a much more dipolar field line. In AM03 both P4 and P5 are close to the plasma sheet center, not to the plasma sheet boundary layer as in T96, and all the spacecraft (except GOES) will map to lower latitudes in the ionosphere in comparison with the T96 model.

4.2. Mapping Issues

4.2.1. Mapping Spacecraft Location to the Ionosphere

[28] Changes in magnetic field configuration shift spacecraft ionospheric footprints. Time variations of spacecraft footprint latitudinal motion are shown in Figure 9 for THEMIS P2 (black), P4 (red), and P5 (blue) and for geostationary GOES 12 (dark green). For comparison, the dashed red line shows the P4 projection according to T96. Horizontal light green and violet lines show the latitudes of the auroral breakup and Gillam observatory, respectively.

[29] One can see that while the P4 footprint changes only slightly according to the T96 model, the AM03 model predicts a significant shift of all THEMIS footprints. During the growth phase they move slowly equatorward by ~1°, followed during the expansion phase by a rapid poleward jump by 2–3°, and finally, a gradual return to ~68° latitude, predicted by the standard T96 model. This type of behavior reminds us of the poleward expansion of the bright auroras during substorms which, to a large extent, can be explained by configurational changes in the magnetic field. This point is further illustrated by Figure 10 in which the latitudinal variations of P4 probe ionospheric footprints, calculated from AM03 model, are superimposed on the auroral keograms (in three wavelengths) from Gillam observatory, as well as on the combined white light keogram from Gillam and Rankin Inlet. Brightenings and poleward jumps of aurora well correlate with the poleward jumps of P4 footprints on Figure 10. We note, in passing, that a similar conjecture, but with respect to inner magnetosphere reconfiguration during strong storms, was made by *Tsyganenko et al.* [2003].

4.2.2. Mapping the Breakup to the Magnetosphere

[30] Luckily, the substorm of 29 March 2009 was not only perfectly covered by spacecraft observations but also provided a set of ground-based auroral data, including an auroral breakup in the central part of the Gillam observatory network, i.e., at the magnetic meridian of THEMIS P4 probe location. Thus, the position of the breakup could be located precisely (see paper 1 for details).

[31] The first brightening signatures were observed at Gillam with exponential brightening occurring at 0517:30 UT. Its position was determined (see paper 1) as 58.7° of geographic latitude and −99.4° longitude or 68.2° of CGL and 2230 MLT.

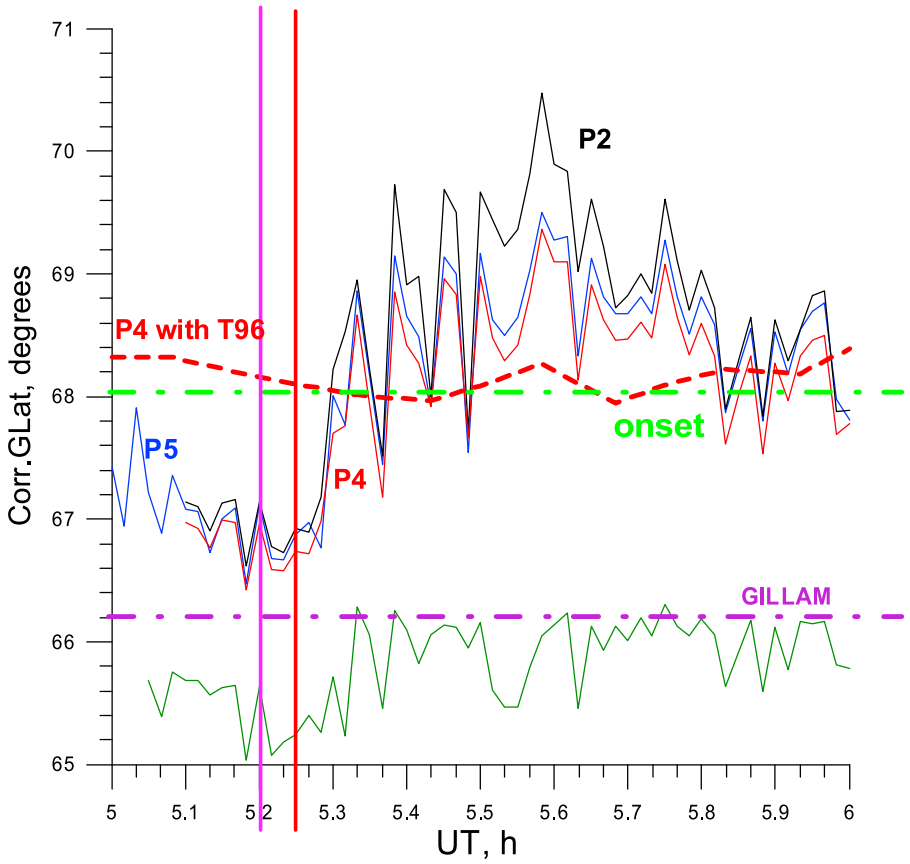

Figure 9. Spacecraft projections time variations for THEMIS probes P2 (black), P4 (red), and P5 (blue) and for geostationary GOES 12 (dark green). The dashed red line shows the P4 projection with T96. Light green and violet horizontal lines show the latitude of a breakup and of Gillam observatory, respectively.

[32] To map the observed breakup to the magnetotail, we calculated mapping curves (CGL against equatorial distance) for the Gillam meridian using both T96 and AM03 models. The result is shown in Figure 11. Two dashed lines, light green and violet, mark the latitudes of onset and of Gillam, respectively. The blue line shows equatorial distances to which the field lines from Gillam magnetic meridian are mapped according to the T96 model. The red and purple lines display the same quantities but obtained with the AM03 model for two UT moments during the late growth phase: the most dipole-like field at 0512 UT and the most stretched configuration at 0515 UT (see Figure 9, in which these two moments are marked by vertical lines of respective color). The difference between the two curves shows the mapping limits, indicating the possible error resulting from the field variability during the late growth phase. Red and blue crosses on both curves show P4 projection to the equatorial neutral sheet for both models, and the triangles indicate the 30 keV proton isotropic boundaries as calculated from both models. The difference in the mapping from the ionosphere to magnetosphere with the two models is very large: for the onset latitude the models give radial distances that differ by about 10 R_E. The AM03 mapping curve starts to significantly deviate from the T96 curve at distances ~10 R_E, where we know, the observed fields at THEMIS locations agree well with the AM03 model, but show much larger discrepancies with the T96.

[33] Additional evidence for the understretched configuration of the magnetic field yielded by the T96 model can be obtained from the analysis of multiple types of observations (paper 1) that place the substorm onset location at 15–20 R_E and certainly tailward from the P2 probe.

4.2.3. Which Model Features Most Influence Mapping?

[34] The main differences between the standard model and the AM03 model are the variable intensity of tail current, the additional neutral sheet rotation in the XZ_{GSM} plane, and the presence of an additional current sheet with variable thickness and intensity. To understand which of these parameters causes larger mapping deviations, we studied several test models in which the parameters of the additional current sheet and the angle of rotation of the entire tail current were varied. The results are shown in Figure 12.

[35] Figure 12 contains the mapping curves corresponding to those in Figure 11 for the AM03 and T96 models plotted in by red and blue. Two other curves were obtained from AM03 by changing only one free parameter at a time within a reasonable range of possible values: in Figure 12a the angle of rotation was changed from −6° (as in a best fit AM03) to −3° and 0°; in Figure 12b the thickness of the additional current sheet was changed from 0.1 R_E to 0.2 R_E and 0.4 R_E (in the T96 model that value was fixed at 2 R_E);

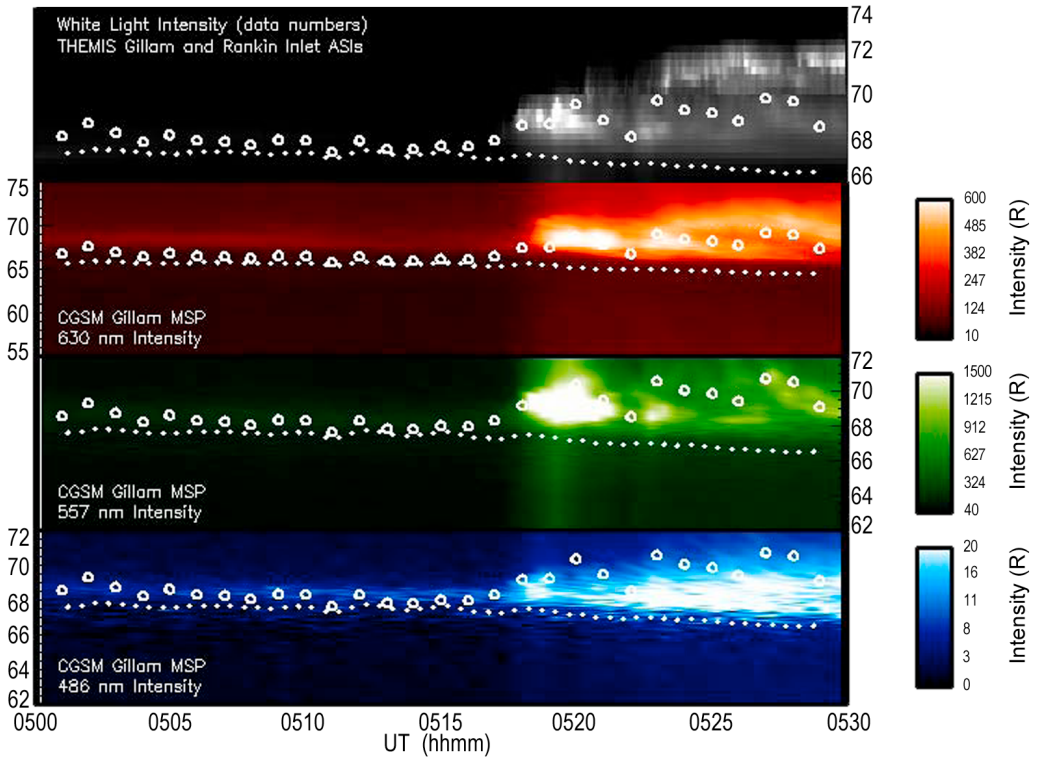

Figure 10. (bottom) Auroral keograms from Gillam observatory (in three wavelengths) and (top) combined white light keogram from Gillam and Rankin Inlet All-Sky Imagers with overplotted P4 probe ionospheric footprints (circles), calculated from AM03 model. Small dots indicate the "optical b2i" boundary positions computed from hydrogen emission data following the *Donovan et al.* [2003] approach.

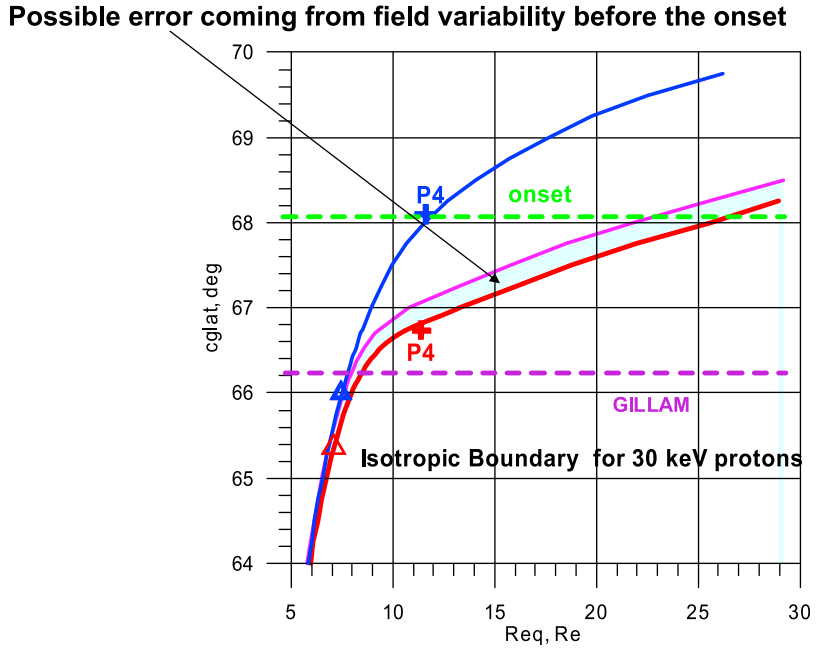

Figure 11. Mapping curves for the Gillam meridian. The blue line shows equatorial distance, to which a field line is mapped from given corrected geomagnetic latitude using the T96 model. Red and purple lines give the same for the AM03 model for two moments of late growth phase, most dipolar configuration at 0512 UT and more stretched 0515 UT (see Figure 9, two moments are marked by vertical lines of corresponding color). Two dashed lines, light green and violet, give the latitudes of onset and Gillam, respectively.

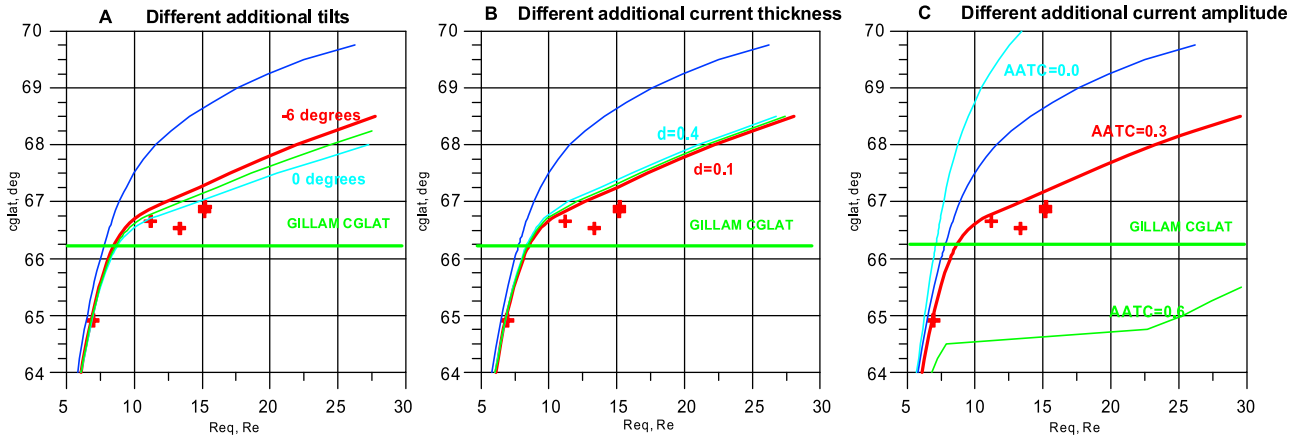

Figure 12. Mapping curves for the T96, AM03, and a number of test models, where free parameters of thin current sheet were varied: (a) the angle of rotation was changed; (b) the thickness of the additional current sheet was changed; and (c) the intensity of the additional current was changed. The blue and red lines are the same as in Figure 11 obtained using the T96 and AM03 models, respectively. The other two curves were obtained using test models.

and in Figure 12c the intensity of the additional current was changed from 30% to 0% and to 60% of the T96 tail current. Here we need to mention that the intensity of main tail current was reduced by 20% in AM03, and that is why the light blue curve in Figure 12c gives a more dipolar mapping curve than in the standard T96 model.

[36] One can see that the most significant changes of mapping curves for test models appear in Figure 12c, where the current intensity was changed; in Figures 12a and 12b the changes of mapping curves for the test models are much smaller. When the tail current becomes more intense, the central part of the mapping curve starting from the equatorial distances ~8–9 R_E flattens (a small step in latitude corresponds to a large change of equatorial footprint tail distance). The stronger the current, the flatter the mapping curve, and the flat part of the curve appears at smaller equatorial distances (see Figure 12c). Therefore, for more intense substorms (and the one we study here is a very moderate one) the mapping curve will be even flatter at the distances 8–20 R_E if compared to the red curve on Figure 10, and the accuracy of the mapping auroral breakups would become questionable.

[37] Thus, we come to a result that makes mapping from ionosphere to magnetosphere very problematic due to existence of a rather flat part on a mapping curve, when a half-degree shift of the footprint latitude in the ionosphere corresponds to a greater than ~5 R_E shift in the neutral sheet. This is the case even for a very moderate substorm. The stronger the tail current at the growth phase, the larger the error of the breakup projection into the tail equatorial plane.

5. Summary and Conclusions

[38] The main goal of this work was to reconstruct the dynamical evolution of the nightside magnetospheric configuration during the moderate substorm of 29 March 2009. Because of the fortuitous arrangement of THEMIS and GOES spacecraft in the same sector 22–23 MLT, and the added flexibility of the AM03 model, we were able to accurately reproduce observed magnetic field variations and to significantly improve the accuracy of mapping between ground-based and space observations, especially just before and after the substorm onset.

[39] This method has two important limitations, both related to spacecraft location. Several spacecraft must be in the same local time sector, and they must be distributed along the magnetotail from 6–7 to 15–20 R_E. Such a configuration is essential to distinguish between different current systems, such as the ring current, the tail current, and the additional thin current sheet. Close MLT spacecraft positions are important because the field sources in the T96 model are symmetric with respect to midnight meridian, while the substorm related currents, including the thin current sheet, can develop in a different local time sector. Since our AM03 model does not include any modification of azimuthal distribution of the T96 currents, it is realistic only in the local time sector in which the observations are made.

[40] The model could be further improved by changing the position of maximum current in the additional current sheet in the x and y directions. More spacecraft data in adjacent local time sectors will be needed to constrain these free parameters, however, and these would be very difficult to obtain, even with THEMIS mission.

[41] In summary, the AM03 model has the following notable features:

[42] 1. The model agrees with observations with much better accuracy than T96, with an average error between 2 and 7 nT during the whole substorm, and the predicted neutral sheet position agrees with the observed one.

[43] 2. The model differs considerably from the standard T96 model during both growth and expansion phases with respect to B values and field line configuration.

[44] 3. Spacecraft footprints obtained with AM03 differ from T96 footprints (which are stable during the whole substorm) by roughly −1.5° of CGL during the growth phase and by up to +2.5° during the expansion phase. Thus,

the overall variability of spacecraft footprints reaches ~4° and resembles typical behavior of the poleward edge of the auroral bulge.

[45] An advantage of the event we studied is that there are extended ground observations at Gillam observatory, including breakup observations in the same local time sector. Thus, the AM03 model may be applied for mapping the breakup from the ionosphere to the magnetospheric neutral sheet. Having compared the mapping results with those obtained using the T96 model, we came to the following conclusions.

[46] 1. Mapping curves are considerably different for the standard and the adapted models (see Figure 10); the difference in equatorial footprint distances increases with latitude and becomes significant (about 10 R_E) for breakup latitudes.

[47] 2. Maximal deviation of the mapping curve from a standard one is obtained close to the distances of maximal current density position (in this event around 10 R_E, where P4 and P5 observations are reproduced by the AM03 model with good accuracy).

[48] 3. Mapping the breakup using standard models results in much smaller equatorial distances than with the more realistic AM03 model, which places breakup into the midtail thin current sheet, in agreement with other observations presented by *Sergeev et al.* [2010].

[49] Conclusion 3 was also obtained in all previous studies, for which the authors used adaptive technique to maximize the agreement of the models with spacecraft observations. These studies concentrated on the late growth phase of substorms with good coverage of the near-tail region, the substorm occurred on 22 March 1975, 19 April 1985, 26 September 2005, 26 April 2009, etc. [see *Pulkkinen*, 1991; *Pulkkinen et al.*, 1991, 1994a, 1995; *Kubyshkina et al.*, 1999, 2002, 2009; *Sergeev et al.*, 2005]. In all previous studies the mapping curves were obtained for the end of the growth phase, and all the curves showed similar features: (1) much more tailward projections for distances beyond 7–10 R_E in comparison with standard T89 and T96 models and (2) the presence of a flat part on the mapping curve where small differences in ionospheric latitude lead to large differences in equatorial distance. For more intensive substorms, the mapping curve flattens, implying even larger (compared to 10 R_E in this study, see Figure 10) differences in the mapping of the breakup to the magnetosphere. As a result, while mapping from magnetosphere to ionosphere may be accurate enough (mapping from the same distance of 10 R_E with T96 and AM03 gives ionospheric difference of ~1° of magnetic latitude), mapping from ionosphere to neutral sheet becomes very unstable, and even small variation of a model will lead to large errors in estimation of radial distance. Thus, determining the equatorial position of ionospheric breakup location using standard model field-aligned mapping can lead to gross errors and wrong interpretation of observations.

[50] **Acknowledgments.** The work was supported by the THEMIS contract NAS5-02099. The work by V.S. and M.K. was also supported by Russian Ministry of Science grants, by the RFBR grant 10-05-91163. H. U. Auster acknowledges financial support by the German Ministerium für Wirtschaft und Technologie and the Deutsches Zentrum für Luft- und Raumfahrt under grant 50QP0402. We thank Judy Hohl for her help in preparing the manuscript.

[51] Masaki Fujimoto thanks Alexander Yahnin and another reviewer for their assistance in evaluating this paper.

References

Auster, H. U., et al. (2008), The THEMIS fluxgate magnetometer, *Space Sci. Rev.*, *141*, 235–264, doi:10.1007/s11214-008-9365-9.

Birn, J., K. Schindler, and M. Hesse (2003), Formation of thin current sheets in the magnetotail: Effects of propagating boundary deformations, *J. Geophys. Res.*, *108*(A9), 1337, doi:10.1029/2002JA009641.

Donovan, E. F., B. J. Jackel, I. Voronkov, T. Sotirelis, F. Creutzberg, and N. A. Nicholson (2003), Ground-based optical determination of the b2i boundary: A basis for an optical MT-index, *J. Geophys. Res.*, *108*(A3), 1115, doi:10.1029/2001JA009198.

Elphinstone, R. D., D. J. Hearn, J. S. Murphree, and L. L. Cogger (1991), Mapping using the Tsyganenko long mognetospheric model and its relationship to Viking auroral images, *J. Geophys. Res.*, *96*, 1467–1480, doi:10.1029/90JA01625.

Hultqvist, B., and G. Gustafsson (1960), On the magnetic time dependence of auroral zone currents, *J. Atmos. Terr. Phys.*, *19*, 246–259, doi:10.1016/0021-9169(60)90047-7.

Kubyshkina, M. V., V. A. Sergeev, and T. I. Pulkkinen (1999), Hybrid input algorithm: An event-oriented magnetospheric model, *J. Geophys. Res.*, *104*(A11), 24,977–24,993, doi:10.1029/1999JA900222.

Kubyshkina, M. V., V. A. Sergeev, S. V. Dubyagin, S. Wing, P. T. Newell, W. Baumjohann, and A. T. Y. Liu (2002), Constructing the magnetospheric model including pressure measurements, *J. Geophys. Res.*, *107*(A6), 1070, doi:10.1029/2001JA900167.

Kubyshkina, M., T. I. Pulkkinen, N. Y. Ganushkina, and N. Partamies (2008), Magnetospheric currents during sawtooth events: Event-oriented magnetic field model analysis, *J. Geophys. Res.*, *113*, A08211, doi:10.1029/2007JA012983.

Kubyshkina, M., V. Sergeev, N. Tsyganenko, V. Angelopoulos, A. Runov, H. Singer, K. H. Glassmeier, H. U. Auster, and W. Baumjohann (2009), Toward adapted time-dependent magnetospheric models: A simple approach based on tuning the standard model, *J. Geophys. Res.*, *114*, A00C21, doi:10.1029/2008JA013547.

Lu, G., N. A. Tsyganenko, A. T. Y. Lui, H. J. Singer, T. Nagai, and S. Kokubun (1999), Modeling of time-evolving magnetic fields during substorms, *J. Geophys. Res.*, *104*(A6), 12,327–12,337, doi:10.1029/1999JA900145.

Pulkkinen, T. I. (1991), A study of magnetic field and current configurations in the magnetotail at time of a substorm onset, *Planet. Space Sci.*, *39*, 833–845, doi:10.1016/0032-0633(91)90088-R.

Pulkkinen, T. I., D. N. Baker, D. H. Fairfield, R. J. Pellinen, J. S. Murphree, R. D. Elphinstone, R. L. McPherron, J. F. Fennell, R. E. Lopez, and T. Nagai (1991), Modeling the growth phase of a substorm using the Tsyganenko model and multi-spacecraft observations: CDAW-9, *Geophys. Res. Lett.*, *18*(11), 1963–1966, doi:10.1029/91GL02002.

Pulkkinen, T. I., D. N. Baker, D. G. Mitchell, R. L. McPherron, C. Y. Huang, and L. A. Frank (1994a), Thin current sheets in the magnetotail during substorms: CDAW 6 revisited, *J. Geophys. Res.*, *99*(A4), 5793–5803, doi:10.1029/93JA03234.

Pulkkinen, T. I., D. N. Baker, P. K. Toivanen, R. J. Pellinen, R. H. W. Friedel, and A. Korth (1994b), Magnetospheric field and current distributions during the substorm recovery phase, *J. Geophys. Res.*, *99*(A6), 10,955–10,966, doi:10.1029/93JA02718.

Pulkkinen, T. I., D. N. Baker, R. J. Pellinen, J. S. Murphree, and L. A. Frank (1995), Mapping of the auroral oval and individual arcs during substorms, *J. Geophys. Res.*, *100*(A11), 21,987–21,994, doi:10.1029/95JA01632.

Pulkkinen, T. I., N. Y. Ganushkina, E. I. Tanskanen, M. Kubyshkina, G. D. Reeves, M. F. Thomsen, C. T. Russell, H. J. Singer, J. A. Slavin, and J. Gjerloev (2006), Magnetospheric current systems during stormtime sawtooth events, *J. Geophys. Res.*, *111*, A11S17, doi:10.1029/2006JA011627.

Sanny, J., R. L. McPherron, C. T. Russell, D. N. Baker, T. I. Pulkkinen, and A. Nishida (1994), Growth-Phase Thinning of the Near-Earth Current Sheet During the CDAW 6 Substorm, *J. Geophys. Res.*, *99*(A4), 5805–5816, doi:10.1029/93JA03235.

Sergeev, V. A., D. G. Mitchell, C. T. Russell, and D. J. Williams (1993), Structure of the tail plasma/current sheet at ~11 R_E and its changes in the course of a substorm, *J. Geophys. Res.*, *98*(A10), 17,345–17,365, doi:10.1029/93JA01151.

Sergeev, V. A., et al. (2005), Transition from substorm growth to substorm expansion phase as observed with a radial configuration of ISTP and Cluster spacecraft, *Ann. Geophys.*, *23*, 2183–2198, doi:10.5194/angeo-23-2183-2005.

Sergeev, V., et al. (2007), Observation of repeated intense near-Earth reconnection on closed field lines with Cluster, Double Star, and other spacecraft, *Geophys. Res. Lett.*, *34*, L02103, doi:10.1029/2006GL028452.

Sergeev, V., V. Angelopoulos, M. Kubyshkina, E. Donovan, X. Zhou, A. Runov, H. Singer, J. McFadden, and R. Nakamura (2010), Substorm growth and expansion onset as observed with ideal ground-spacecraft THEMIS coverage, *J. Geophys. Res.*, *116*, A00I26, doi:10.1029/2010JA015689.

Tsyganenko, N. A. (1989), Magnetospheric magnetic field model with a warped tail current sheet, *Planet. Space Sci.*, *37*, 5–20, doi:10.1016/0032-0633(89)90066-4.

Tsyganenko, N. A. (1995), Modeling the Earth's magnetospheric magnetic field confined within a realistic magnetopause, *J. Geophys. Res.*, *100*(A4), 5599–5612, doi:10.1029/94JA03193.

Tsyganenko, N. A. (2002a), A model of the near magnetosphere with a dawn-dusk asymmetry: 1. Mathematical structure, *J. Geophys. Res.*, *107*(A8), 1179, doi:10.1029/2001JA000219.

Tsyganenko, N. A. (2002b), A model of the near magnetosphere with a dawn-dusk asymmetry: 2. Parameterization and fitting to observations, *J. Geophys. Res.*, *107*(A8), 1176, doi:10.1029/2001JA000220.

Tsyganenko, N. A., and D. H. Fairfield (2004), Global shape of the magnetotail current sheet as derived from Geotail and Polar data, *J. Geophys. Res.*, *109*, A03218, doi:10.1029/2003JA010062.

Tsyganenko, N. A., H. J. Singer, and J. C. Kasper (2003), Storm-time distortion of the inner magnetosphere: How severe can it get?, *J. Geophys. Res.*, *108*(A5), 1209, doi:10.1029/2002JA009808.

Wanliss, J. (2006), Substorm onset location and dipole tilt angle, *Ann. Geophys.*, *24*, 577–588, doi:10.5194/angeo-24-577-2006.

V. Angelopoulos and A. Runov, Institute of Geophysics and Planetary Physics, University of California, Box 951567, Los Angeles, CA 90095, USA.

U. Auster, Institut für Geophysik und Extraterrestrische Physik der Technischen Universitaet Braunschweig, Mendelssohnstrasse 3, D-38106 Braunschweig, Germany.

W. Baumjohann, Space Research Institute, Austrian Academy of Sciences, Schmiedlstrasse 6, A-8042 Graz, Austria.

E. Donovan, Department of Physics and Astronomy, University of Calgary, Calgary, AB T2N 1N4, Canada.

M. Kubyshkina, V. Sergeev, and N. Tsyganenko, Institute of Physics, Saint Petersburg State University, St. Petersburg 198504, Russia. (kubysh@geo.phys.spbu.ru)

H. Singer, NOAA Space Weather Prediction Center, 325 Broadway, Boulder, CO 80303, USA.